Journal of *Marine Science and Engineering*

MDPI

Article

Remote Sensing Monitoring of Green Tide Disaster Using MODIS and GF-1 Data: A Case Study in the Yellow Sea

Yanzhuo Men [1], Yingying Liu [1], Yufei Ma [1], Ka Po Wong [2], Jin Yeu Tsou [3] and Yuanzhi Zhang [1,3,*]

[1] College of Marine Science, Nanjing University of Information Science and Technology, Nanjing 210044, China; 20211237015@nuist.edu.cn (Y.M.); 20211109004@nuist.edu.cn (Y.L.); 20201237008@nuist.edu.cn (Y.M.)
[2] Department of Applied Social Sciences, The Hong Kong Polytechnic University, Hong Kong 999777, China; portia.wong@polyu.edu.hk
[3] Department of Architecture and Civil Engineering, City University of Hong Kong, Hong Kong 999777, China; jytsou@cityu.edu.hk
* Correspondence: yzhang209@nuist.edu.cn

Abstract: Satellites with low-to-medium spatial resolution face challenges in monitoring the early and receding stages of green tides, while those with high spatial resolution tend to reduce the monitoring frequency of such phenomena. This study aimed to observe the emergence, evolution, and migratory patterns of green tides. We integrated GF-1 and MODIS imagery to collaboratively monitor the green tide disaster in the Yellow Sea during 2021. Initially, a linear regression model was employed to adjust the green tide coverage area as captured using MODIS imagery. We jointly observed the distribution range, drift path, and coverage area of the green tide and analyzed the drift path in coordination with offshore wind field and flow field data. Furthermore, we investigated the influence of SST, SSS, and rainfall on the 2021 green tide outbreak. The correlations calculated between SST, SSS, and precipitation with the changes in the area of the green tide were 0.43, 0.76, and 0.48, respectively. Our findings indicate that the large-scale green tide outbreak in 2021 may be associated with several factors. An increase in SST and SSS during the initial phase of the green tide established the essential conditions, while substantial rainfall during its developmental stage provided favorable conditions. Notably, the SSS exhibited a close association with the outbreak of the green tide.

Keywords: green tide; GF-1; MODIS; the Yellow Sea

Citation: Men, Y.; Liu, Y.; Ma, Y.; Wong, K.P.; Tsou, J.Y.; Zhang, Y. Remote Sensing Monitoring of Green Tide Disaster Using MODIS and GF-1 Data: A Case Study in the Yellow Sea. *J. Mar. Sci. Eng.* **2023**, *11*, 2212. https://doi.org/10.3390/jmse11122212

Academic Editor: Aurélie Blanfuné

Received: 30 September 2023
Revised: 7 November 2023
Accepted: 17 November 2023
Published: 22 November 2023

1. Introduction

The term green tide refer to the excessive growth and aggregation of macroalgae under specific environmental conditions, such as effluent discharge from aquaculture and eutrophication of water bodies [1,2]. Globally, green tides have become a serious marine environmental issue. Over the past few decades, their frequency and scale have progressively increased, exerting widespread adverse effects on marine ecosystems, fisheries, tourism, and human activities [3,4].

The Yellow Sea region is one of the areas most frequently afflicted by green tides, particularly during the summer seasons in recent years [5]. The monitoring and management of green tides have, thus, become paramount. While on-site measurements can be conducted using ships, the limited number of measurement points makes it challenging to grasp the distribution and changes in the extent of green tides [6]. Satellite remote sensing data, which is easy to obtain and offers a wide coverage, is increasingly used for monitoring large phytoplankton events such as green tide disasters [7]. Different remote sensing data possess varying spatiotemporal resolutions. High spatial resolution data allows for more precise monitoring of targets, while high temporal resolution data facilitates continuous, real-time monitoring. Thus, when extracting green tide information, selecting the most appropriate remote sensing imagery based on spatial scale has practical significance and application value [8]. Some studies have shown that 250 m resolution

MODIS data tends to overestimate when extracting the coverage area of green tides, with the monitored coverage area being two to three times the actual value [9]. This is because low-resolution remote sensing data, such as MODIS and GOCI, struggle to capture fine details of the ocean surface while covering the entire study area, resulting in a significant number of mixed pixels [2,4,10]. Additionally, wide-swath images covering the study area offer enhanced monitoring capabilities for target regions. Given current remote sensing technologies, there exists an irreconcilable contradiction between spatial resolution and swath width: high-resolution data tend to have a narrow swath. When the swath is too narrow, the images lose their utility for operational monitoring of green tides [11]. Hence, combining high spatial resolution with wide swath and high temporal resolution images for monitoring green tide disasters holds significant research value.

Numerous studies have already explored the extraction of information, drift paths, and outbreak causes of green tides. For instance, Klemas discussed the application of satellite data like AVHRR, SeaWiFS, and MODIS for global green tide monitoring [12]. Wu et al. indicated, based on satellite remote sensing data, that the seasonal warming in the southwestern Yellow Sea plays a crucial role in the late spring and early summer green tide outbreaks [13]. Ma et al. combined MODIS and SAR remote sensing data to analyze the temporal and spatial characteristics of the 2021 Yellow Sea green tides. Compared to solely using a single data source, this combination increased the frequency of temporal observations [14]. Yang et al. utilized the HY-1C/Coastal Zone Imager (HY-1C/CZI) and the Terra/MODIS satellite imagery to extract the spatiotemporal distribution of the floating green tide in the Yellow Sea in 2019. A comparison was made between the green tide areas extracted from the two types of images. The spatial resolution of the CZI is 50 m (0.0025 km^2), while that of MODIS is 250 m (0.0625 km^2). It was observed that when the green tide area is small, MODIS struggles to detect patches smaller than its spatial resolution. When the green tide patches are less than 11.2 km^2, the area extracted using Terra/MODIS tends to be underestimated. On the other hand, when the green tide area is large, the lower spatial resolution of MODIS results in a larger proportion of mixed pixels between water and algae, leading to an overestimation of the total green tide area [15].

Understanding the factors influencing the formation of green tides is crucial for their prediction and control. The green tides in the Yellow Sea, being of the floating type, are jointly affected by winds and surface currents [16]. Numerical simulation studies also suggest that wind and currents are the primary drivers of the northward drift of green tides [17]. Cao et al. used GF1-WFV and GOCI images to analyze the influence of typhoon "Chan-hom" on the growth and drift path of green tides [18]. Li et al. found that the initial size of the green tides does not directly impact the outbreak scale. However, lower sea surface temperatures (SST) and adequate precipitation in the early stages might foster large-scale occurrences [19]. Li et al. assessed green tides from 2007 to 2021 and the long-term trends of various factors influencing them over the past 30 years. The study revealed the combined promoting effects of SST, nutrient pollution, and "nori" cultivation on green tide outbreaks, as well as the impacts of environmental factors like SST, sea surface salinity (SSS), and radiation [20]. SST and precipitation influence the dissipation time of green tides; higher temperatures speed up the dissipation process, while precipitation slows it down [21].

Previous studies on the remote sensing monitoring of green tides primarily utilized single data sources. Alternatively, they combined various imaging results to extend the monitoring timeframe. However, the varied resolution of different remote sensing images affects the analysis of the results. Moreover, low-resolution remote sensing data have significant errors in monitoring the area of green tides [12–14]. Consequently, this study employed both GF-1 and MODIS remote sensing data. The GF-1 data have a high spatial resolution of 16 m, but few studies have utilized GF-1 for green tide monitoring. In contrast, many studies focusing on green tide monitoring opt for MODIS data. Although MODIS images have a wider swath that can fully cover green tide disaster areas and feature high temporal resolution, their lower spatial resolution introduces considerable errors in

monitoring the area of green tides [2,4,10,11,15]. In this study, the green tide area detected in GF-1 data was used to correct the green tide area in MODIS images, enhancing the accuracy of MODIS image monitoring of green tide areas. By leveraging the strengths of both images, a more accurate monitoring of green tide disasters was achieved. This study focuses on the monitoring of the 2021 Yellow Sea green tide, utilizing both GF-1 and MODIS images to observe the distribution, drift paths, and covered areas during the 2021 green tide. By also considering environmental factors such as SST, SSS, precipitation, sea surface wind fields, and flow fields, this research explored the mechanisms behind the outbreak of the 2021 green tide disaster, offering support for studies on green tide disaster monitoring using satellite images of different resolutions.

2. Materials and Methods

2.1. Study Area

The focal region of this study is the Yellow Sea, situated between 31°–37° N and 119°–124° E, as delineated in Figure 1. Occupying a premier position as the largest marginal sea of the Pacific Ocean, the Yellow Sea is subjected to the perennial influence of monsoon winds. Commencing in May, a southward monsoon initiates, giving way to predominant south to southeast winds from June through to August. The monsoon season extends from June to September, during which time over half of the annual precipitation is received. The unique combination of the Yellow Sea's natural geographical characteristics and climatic factors induces a stable aquatic environment, thereby favoring the genesis and proliferation of large floating algae such as seaweed.

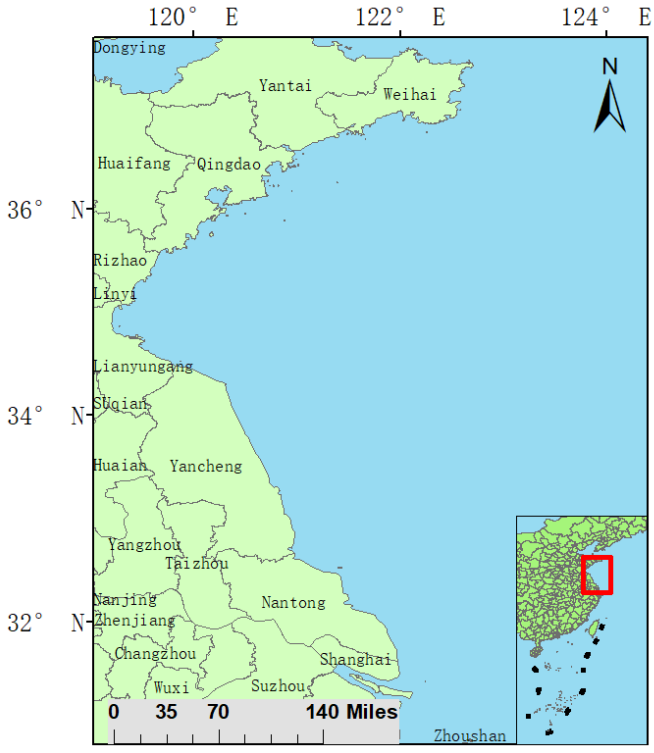

Figure 1. The Yellow Sea (31°–37° N, 119°–124° E).

2.2. Dataset

The GF-1 Wide Field Imager satellite data utilized in this research were sourced from the China Resources Satellite Application Center (https://data.cresda.cn (accessed on 8 May 2022)). These data offer a spatial resolution of 16 m and a revisit interval of four days. The GF -1 data have advantages in monitoring small-area green tides [22,23], and consequently, the GF-1 imagery data have made a significant contribution to the research on green tide monitoring [24–26]. The moderate-resolution imaging spectroradiometer

(MODIS) data, obtained from NASA (https://ladsweb.modaps.eosdis.nasa.gov (accessed on 8 May 2022)), have a spatial resolution of 250 m (for bands 1–2) and an extensive swath width of 2330 km, enabling the acquisition of daily satellite images. Table 1 shows the wavelength ranges of GF-1 and MODIS.

Table 1. Wavelength ranges of GF-1 and MODIS.

Satellite	Band Order	Wavelength (nm)
GF-1 WFV	1	450–900
	2	450–520
	3	520–590
		630–690
MODIS	1	620–670
	2	841–876

Wind field data, SST, and total precipitation data were gathered from the ECMWF 5th generation atmospheric reanalysis global climate dataset (ERA5) (https://cds.climate.copernicus.eu/ (accessed on 8 May 2022)), offering a spatial resolution of 0.25° × 0.25°. The sea current data were procured from the Copernicus Ocean Observing Service (COOS), which offers a standard grid with a spatial resolution of 1/12° and a temporal resolution of one day (https://marine.copernicus.eu/ (accessed on 8 May 2022)). Additionally, SSS data were obtained from SMAP (soil moisture active passive) satellites, which provide global coverage in an 8-day cycle (https://www.remss.com/missions/smap/salinity/ (accessed on 8 May 2022)).

Data on daily precipitation and SST from 1 May to 30 June 2021 were acquired. Additionally, daily sea surface current and wind field data from 22 May to 8 August 2021 were obtained. Concurrently, data on SST, SSS, and total precipitation for the period from April to June 2021 were also collected.

2.3. Data Preprocessing

In this study, both GF-1 and MODIS imagery underwent a series of preprocessing steps, including radiometric calibration, atmospheric correction, geometric rectification, land–water discrimination, image cropping, and stitching. Following these adjustments, the normalized difference vegetation index (NDVI) was employed to extract information about the green tide; the threshold values utilized for the extraction of green tide information from GF-1 and MODIS images ranged from 0 to 0.18. For the calculation of MDVI, the third and fourth bands of GF-1 were used, as well as the first and second bands of MODIS. To construct a linear fitting model between GF-1 and MODIS imagery, the images were scrutinized and cropped, ensuring temporal and spatial consistency across the scope of the study.

2.4. Methods

Green tide extraction from remote sensing images in our research utilizes a distinct feature of green tide: it exhibits low reflectivity in the visible band and high reflectivity in the near-infrared band. This enables us to monitor green tide-related hazards effectively. In 1973, the concept of the normalized vegetation index (NDVI) was introduced by Rouse et al., based on the principle that the concentration of chlorophyll in a body of water serves as an indicator of algal presence [27]. The definition of the NDVI is as follows:

$$NDVI = \frac{R_{NIR} - R_{RED}}{(R_{NIR} + R_{RED})} \quad (1)$$

where R_{NIR} denotes the reflectance in the near-infrared band and R_{RED} refers to the reflectance in the red light band. If the value of the *NIR* band is less than that of the red light band, the *NDVI* is less than 0. Conversely, as the content of chlorophyll in waters

with algal presence increases, causing the value of the NIR band to exceed that of the red light band, the *NDVI* will be greater than 0. This principle enables the differentiation between areas with high algal content and non-algal waters. Many studies currently utilize NDVI to extract macroalgae from remote sensing imagery [2,28]. The normalized difference vegetation index (NDVI) has been proven to be an effective indicator for monitoring green tides and has been extensively applied in previous studies [29,30]. Regarding the application of NDVI to the study of green tides in the Yellow Sea, Sakib et al. compared the effects of using NDVI to detect macroalgae in the Yellow Sea between GOCI and Landsat-8, finding that Landsat provides a more significant result when using NDVI to identify macroalgae [31]. Wang et al. utilized NDVI to extract green tides in the Yellow Sea and integrated multi-source data results to monitor the disaster of green tides in the Yellow Sea [32].

3. Results

3.1. MODIS Green Tide Area Correction

Past research has revealed that the green tide coverage area extracted from MODIS data is approximately twice that of the actual value [9]. To fulfill the demands of operational green tide monitoring, the green tide area monitored using high spatial resolution data may be regarded as the actual value, and the corresponding area derived from low-resolution images can be adjusted [33]. In the present study, GF-1 and MODIS images dated 10 July 2021 were processed in segments and divided into numerous 100-pixel by 100-pixel sample blocks. Within each sample block, the green tide coverage area in both the GF-1 and MODIS images was quantified and a linear relationship was constructed between the green tide coverage areas in the sample blocks of the two images. This process was undertaken to fine-tune the green tide coverage area of the MODIS image, thereby refining the monitored green tide area.

Upon comparing the images shown in Figure 2b,c, it becomes apparent that the shapes of the green tide patches in both the GF-1 and MODIS images within identical sample blocks are alike. However, due to variations in spatial resolution between the two images, certain small green tide patches found in the GF-1 image sample blocks are absent in the MODIS counterparts. Conversely, the proportion of the area covered by larger green tide patches within identical sample blocks is greater in the GF-1 image than in the MODIS image.

By treating the GF-1 and MODIS sample blocks within the same region as a group and excluding sample block groups with an area of zero, a linear fit was performed between the sample blocks of the two images. The results are depicted in Figure 2d. Consequently, the linear relationship model between the GF-1 and MODIS images was established as follows: (The model would follow in the text).

$$y = 1.43x + 230.86 \quad (2)$$

The linear fitting of the green tide covered areas in the GF-1 and MODIS images yielded a determination coefficient (R^2) of 0.83, indicating a strong fit. For the green tide areas extracted from GF-1 and MODIS images over the same time range, Formula (2) can be used to convert the green tide area in the MODIS images, and Formula (3) can be applied to calculate the relative error value after the conversion of the MODIS image.

$$\left(\frac{area\ in\ the\ transformed\ MODIS\ imagery\ -\ area\ in\ the\ concurrent\ GF-1\ imagery}{area\ in\ the\ concurrent\ GF-1\ imagery}\right) \times 100\% . \quad (3)$$

The GF-1 and MODIS images from 8 June 2019, 3 July 2019, and 20 June 2021 were selected to validate the model. As shown in Table 2, the results indicate that the error value between the green tide cover areas monitored using MODIS and GF-1 images remains within 15%.

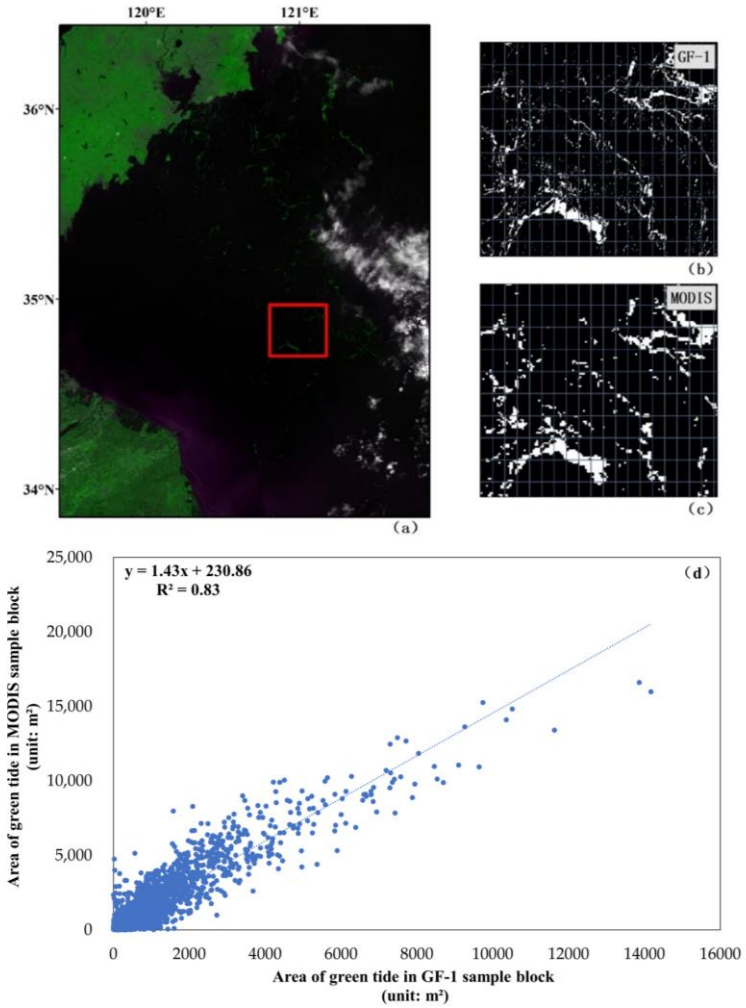

Figure 2. (**a**) is the true color image of GF-1 image, the red square represents a selected area within the range of the green tide. (**b**,**c**) are the segmentation diagrams of GF-1 image and MODIS image, respectively, and (**d**) is the relationship model of green tide coverage area of the two images.

Table 2. Linear fitting model validation.

Satellite	Time	Pixel Size (m)	Number of Pixels	Area (km^2)	MODIS Converted Area (km^2)	Error
GF-1	8 June 2019	19 × 19	1,766,965	637.87	-	-
	3 July 2019	18 × 18	1,795,157	581.63	-	-
	20 June 2021	19 × 19	2,278,052	822.38	-	-
MODIS	8 June 2019	250 × 250	15,952	997	696.03	9.12%
	3 July 2019	250 × 250	15,264	954	666.015	14.51%
	20 June 2021	19 × 19	3,671,233	1325.32	925.24	12.51%

3.2. Analysis of the Green Tide Drift Path and Influencing Factors in 2021

In this research, GF-1 and MODIS remote sensing images were meticulously selected from the Yellow Sea region, focusing on those with cloud cover less than 10% and containing discernible green tide. This selection enabled the mapping of the green tide distribution range for the period between May and August 2021, as illustrated in Figure 3. During the initial stages of green tide outbreaks, *Sargassum* sp often appears concomitantly with *Ulva clathrata* prolifera. It is documented that algae outbreaks tend to peak from mid- to late May. Furthermore, the algae found in the southern Yellow Sea waters before 13 May were

primarily *Sargassum* sp., those after 5 June were predominantly seagrass, and a composite mixture of *Sargassum* sp. and *Ulva clathrata* prolifera was observed to grow between 13 May and 4 June [34,35].

Figure 3. Distribution range of green tide from May to August 2021.

The spatial distribution of the green tide from May through to August was closely analyzed and visualized (Figure 4a,b). During the May–June phase, the extent of the area covered by the green tide demonstrated a gradual expansion, drifting from Jiangsu to Qingdao in Shandong Province. In the subsequent period of July–August, the green tide's distribution stabilized and was primarily confined to the coastal waters of Qingdao.

Utilizing the mean center tool within ArcGIS10.7, the central position of the green tide was computed for each image, enabling the delineation of the drift path from the onset to the dissipation of the green tide (Figure 4c). A notable observation was the green tide's proximity to Yancheng City, where the outer edge reached a minimum distance of 24 km on 22 May. In early June, the green tide began its approach towards the coast, with the outer edge coming within 54 km of Qingdao's coastline. This convergence towards the coast of Qingdao persisted through late June and early August. During the initial stages of the green tide, its drift speed was relatively high; however, as the phenomenon developed, both the speed and distance of drift began to decrease progressively.

The origin of the green tide is not the ultimate outbreak area. The green tide, which commenced in May on the shallow shores of northern Jiangsu [9,30], subsequently drifted northward, driven by monsoons and surface currents, ultimately reaching Shandong [9,17]. The drift direction of the green tide is principally aligned with the angle constituted by the surface winds and the sea surface circulation direction, and the trajectory of the green tide's dense region is largely congruent with the prevailing winds [36]. Figure 5 elucidates the daily fluctuations of sea surface winds and currents in the northern Yellow Sea from 22 May to 8 August 2021. When juxtaposed with the drift path of the green tide for the same year, it is discernible that during May through August, the predominant winds in

the northern Yellow Sea were southerly, while the currents exhibited a northerly direction. This alignment is consistent with the green tide's drift path from south to north.

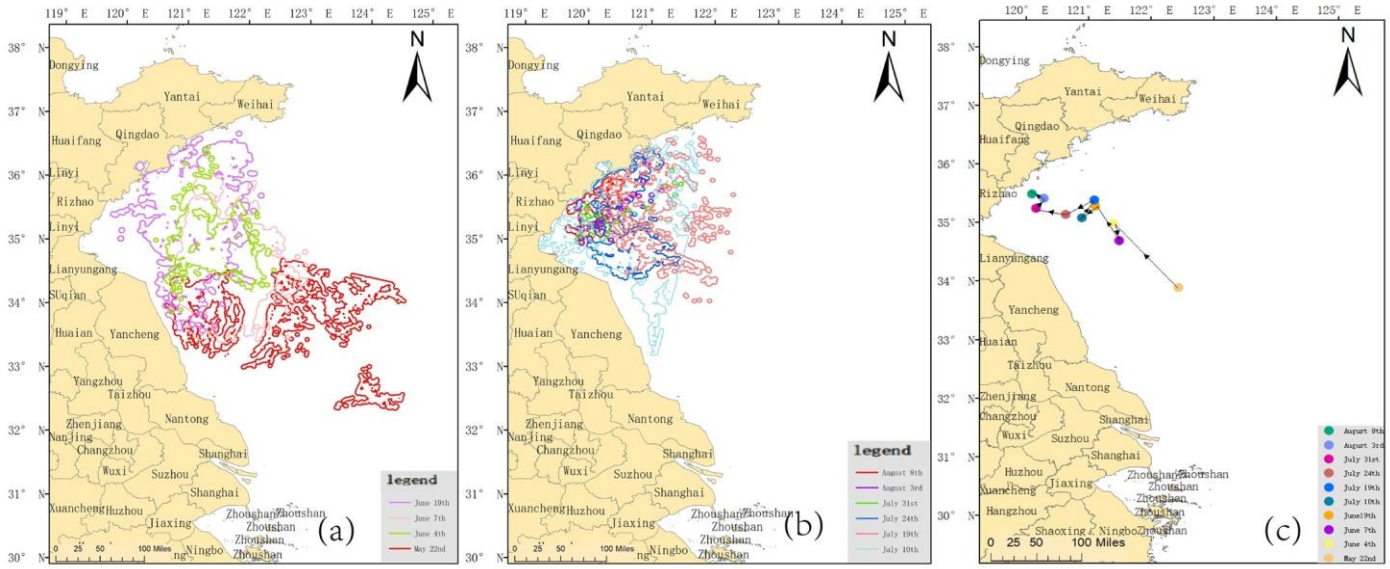

Figure 4. Distribution range of green tides in May–June (**a**), July–August (**b**), and drift path (**c**), 2021.

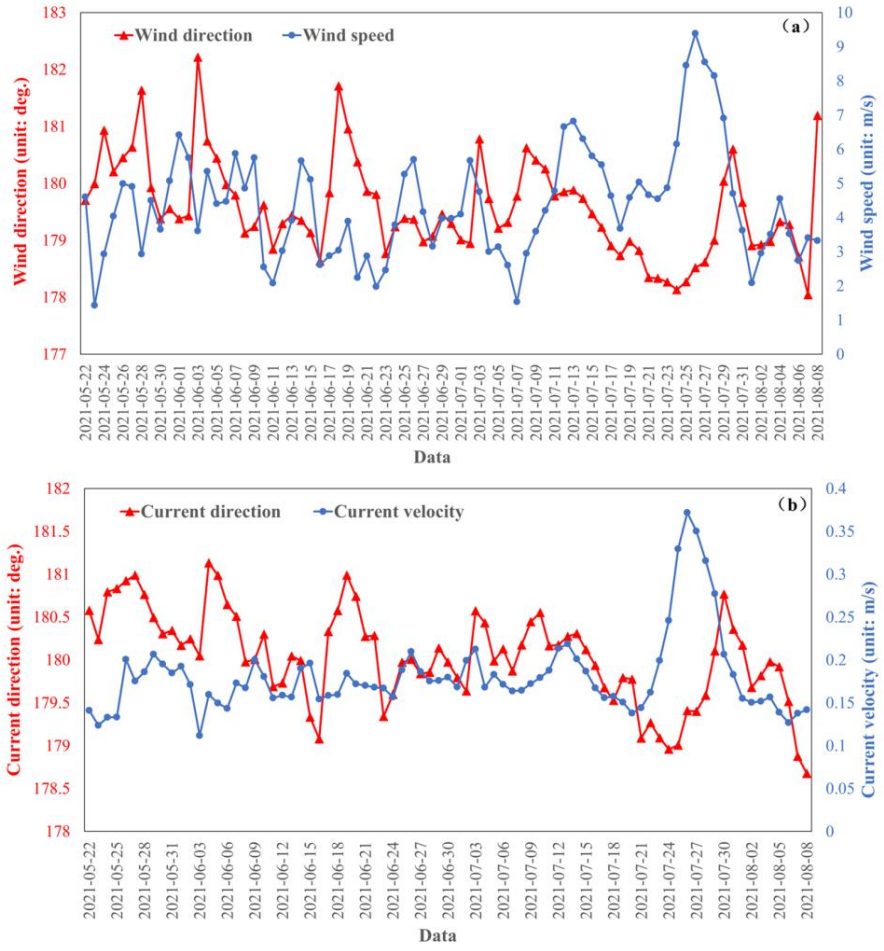

Figure 5. Diurnal variation in sea surface wind (**a**) and current (**b**) in the Yellow Sea from 22 May to 8 August 2021.

In the May–June timeframe, the average wind speed in the green tide region was 5 m/s. During the latter part of May and the early part of June, the green tide was in its incipient stage and consisted predominantly of scattered patches, resulting in a relatively rapid drift speed. However, the drift speed of the green tide began to decelerate from mid-to late June through to the onset of July. Toward the end of July, under the influence of Typhoon "Yuhua," the average wind speed from the south escalated to 9 m/s, accompanied by a robust northward current, propelling the green tide in a northwestward direction. In early August, both wind speed and current velocity were diminished in the Yellow Sea, culminating in the green tide's stabilization in the offshore areas of Qingdao.

Based on the linear fitting model, the area enveloped by the green tide during the outburst period was ascertained by converting the MODIS data, facilitating an examination and analysis of the temporal changes in the green tide's spatial extent (Table 3). On 22 May, the green tide encompassed an area of 82.29 km^2, subsequently experiencing a rapid expansion in early June, with an average daily increase surpassing 50 km^2. A drastic reduction in the green tide's area was observed at the onset of July, culminating in a contraction to 15.29 km^2 in early August.

Table 3. The area of green tide extracted from GF-1 images and MODIS images from May to August 2021. The area detected using GF-1 does not need to be converted, "\" represents the result detected using GF-1.

Time	Satellite	Coverage Area (km^2)	Coverage Area in Converted MODIS Images (km^2)
22 May	GF	82.29	\
4 June	MODIS	1406.63	820.84
7 June	GF	1371.89	\
19 June	MODIS	2766.06	1776.88
10 July	GF	611.35	\
19 July	MODIS	310.56	55.64
24 July	MODIS	440.06	146.05
31 July	MODIS	26.25	\
3 August	MODIS	21.00	\
8 August	GF	15.11	\

This considerable contraction in the early part of July was correlated with a decrease in the area of the green tide to 15.5 km^2. According to the documented evidence, the Qingdao government orchestrated an extensive and concerted effort to intercept and manage the green tide at sea in July, deploying 17,537 fishing vessels, installing 266,900 m of interception nets, and salvaging 741,300 tons of seashore moss [37]. When viewed in conjunction with the monitoring data, these actions corroborate that the Qingdao government's timely implementation of salvage measures effectively accelerated the attenuation of the green tide, thus, underscoring the importance of coordinated and proactive management in mitigating the impact of this environmental phenomenon.

3.3. Causes of Large-Scale Green Tide Outbreaks in 2021

Table 4 presents the statistical findings, as detailed in the China Marine Disaster Bulletin [38], concerning the occurrence of green tides in the Yellow Sea from 2012 to 2021. A discernible observation from these data reveals that the green tide outbreak in 2021 constitutes the most severe incident within this time frame, surpassing previous years in both maximum distribution area and maximum coverage area [39]. Within the period studied in this paper, the maximum area of the green tide outbreak aligns with the officially announced maximum extent. This further substantiates the feasibility of the method combining MODIS and GF-1 imagery for the inversion of green tide. Past research indicates that the emergence and evolution of the green tide in the Yellow Sea are primarily influenced by climate change and human intervention [40]. The growth of the green tide is impacted by various factors. Salinity, temperature, nutrients, light, and

pH levels exert significant effects on algal growth [41–43]. An appropriate temperature can enhance algal proliferation [44]. Similarly, different salinity levels result in diverse algal growth conditions. When seawater salinity is relatively high (>30‰), it favors algal reproduction [42]. Thus, when *Ulva clathrata* enters open waters with a salinity level > 31‰, it further promotes rapid proliferation [45]. However, excessively high or low salinity can inhibit the outbreak of the green tide. Extreme precipitation events also affect the growth of the green tide [42,43]. Extreme precipitation events can also impact the growth of green tide. Precipitation not only promotes the deposition of atmospheric nutrients but also intensifies the marine convection. This results in the upward transport of nutrients from the seabed to the surface, leading to alterations in the surface nutrient concentration, thereby exacerbating the development and expansion of the green tide [46]. The subsequent sections of this paper will provide an in-depth analysis of the oceanic conditions (SST, SSS, and precipitation levels) during the preliminary and developmental phases of the green tide (from April to June 2021). The aim is to elucidate the mechanisms underlying the massive outbreak of the green tide in 2021. Subsequent sections of this paper will delve into an analysis of sea surface conditions during both the pre-green tide period and the development phase of the green tide (namely, April to June 2021), to elucidate the causal mechanisms underlying the large-scale outbreak of the green tide in 2021.

Table 4. Occurrence of green tide in the Yellow Sea area of China from 2012 to 2021.

Year	The Earliest Discovery Time	Extinction Time	Maximum Distribution Area (km^2)	Maximum Coverage Area (km^2)
2012	Mid to late May	Late August	19,610	267
2013	Mid May	Mid August	29,733	790
2014	Mid May	Mid August	50,000	540
2015	Mid to late May	Early August	52,700	594
2016	Early May	Early August	57,500	554
2017	Mid May	Mid to late July	29,522	281
2018	Late May	Mid August	38,046	193
2019	Mid to late May	Early September	55,699	508
2020	Late May	Late July	18,237	192
2021	Mid May	Late August	61,898	1746

Utilizing the monthly average data acquired from ERA5 and COOS, the distribution maps of SST, SSS, and precipitation for the Yellow Sea region during the months of April to June 2021 were produced (Figure 6). As is evident from Figure 6, within the latitude range of 31° N to 37° N and longitude range of 120° E to 124° E, the SST in April was relatively low, remaining below 15 °C. In April, the SST registered a low, falling below 15 °C, then incrementally rose during May and June, attaining peak temperatures of approximately 20 °C in May and around 25 °C in June. A comparative analysis indicates that the SST in the southern Yellow Sea exceeds that in the northern region, with a gradual temperature decrease observed from south to north. During April to June, the northern Yellow Sea (especially in the Yancheng and Weihai) generally has a higher SSS, averaging around 30‰, and can reach up to 32‰. The salinity values in the northern Yellow Sea from April to June are above 30‰, which falls within the salinity range that promotes algal growth [42]. Concurrent meteorological reports highlight the appearance of a temperate cyclone in Jiangsu Province in late April and early May, accompanied by medium to large wave formations in the southern Yellow Sea and northern East China Sea. Measurements indicated peak effective wave heights of 1.8 m and maximum wave heights of 2.8 m in the southern Yellow Sea [38]. Additionally, areas of intensified rainfall were detected across the study seas in May and June, with precipitation exceeding 250 mm in the northern waters of the Yellow Sea in June. Based on the observed phenomena, we calculated the Pearson correlation between the changes in green tide area and three natural factors: SST, SSS, and precipitation, with results of 0.43, 0.76, and 0.48, respectively. It can be observed that the

correlation between salinity and green tide area is the highest. Therefore, the increase and decrease in the area of green tide in 2021 is closely related to changes in salinity.

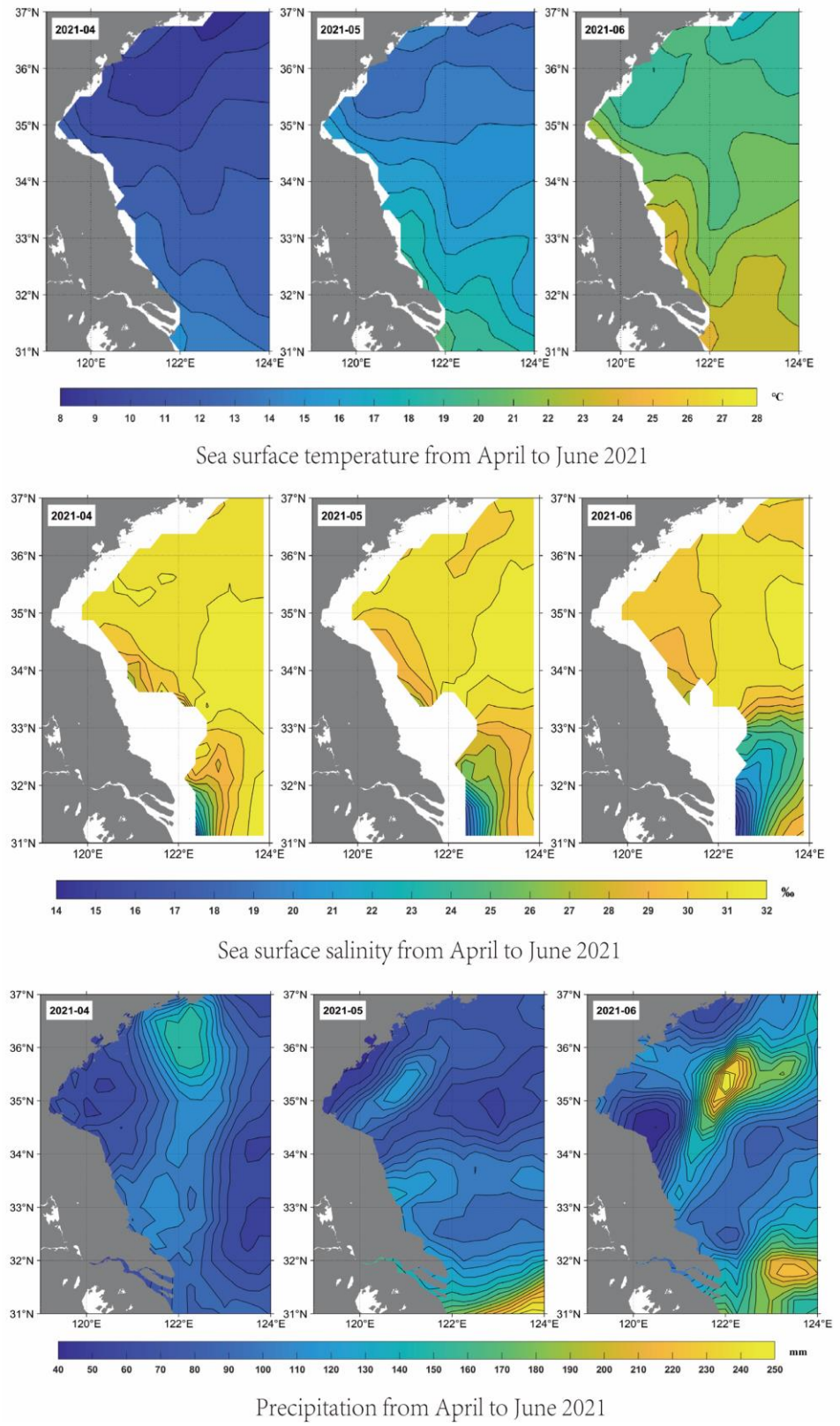

Figure 6. Monthly mean SST, SSS, and precipitation from April to June 2021.

A comparison of the SST, SSS, and precipitation in 2021 with the corresponding multi-year averages reveals distinct anomalies (Figure 7). Specifically, the SST within the coordinates of 31°N–35°N and 120°E–124°E for the period from April to June 2021 was observed to be elevated in comparison to the mean temperature of previous years. Concentrated regions of heightened SST were notably present in the offshore waters of Lianyungang in both April and June. Moreover, a comprehensive analysis of SSS during April and May in the Yellow Sea, particularly in the northern offshore waters spanning Lianyungang to Rizhao, indicated values exceeding those recorded in prior years. A salient observation warrants attention, namely, that the monthly precipitation levels for 2021 within the geographical bounds of 33° N–37° N and 120° E–124° E were found to be significantly higher than those in preceding years.

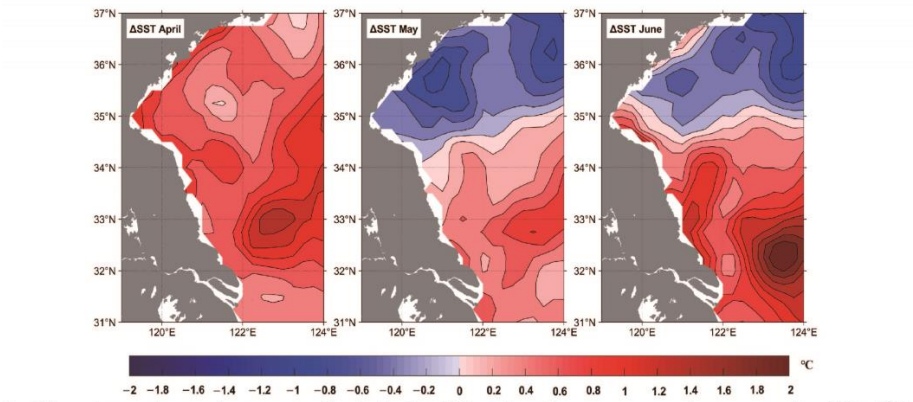

The difference between the sea surface temperature from April to June 2021 and the multi-year average sea surface temperature from 2012 to 2021

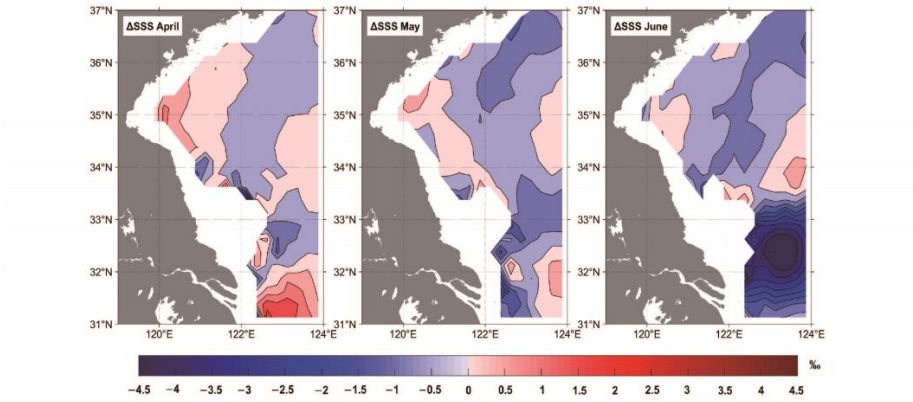

The difference between the sea surface temperature from April to June 2021 and the multi-year average sea surface salinity from 2012 to 2021

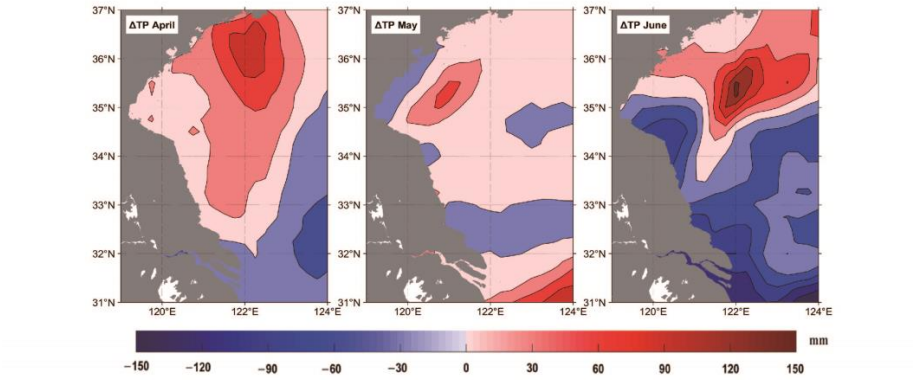

The difference between the sea surface temperature from April to June 2021 and the multi-year average sea surface precipitation from 2012 to 2021

Figure 7. The difference between SST, SSS, and precipitation in 2021 and the average SST, SSS (2015–2021), and precipitation in 2012–2021.

Furthermore, experimental evidence has elucidated that the water temperature range of 10 °C to 25 °C is most conducive to seaweed growth, with the optimal growth rate being observed within the temperature bracket of 15 °C to 20 °C, and the most favorable temperature for germination identified as 20 °C [20,47]. A more granulated examination of the daily precipitation and SST during May and June in the region susceptible to green tide outbreaks in the Yellow Sea (coordinates 34° N–37° N, 119° E–122° E) for 2021 reveals a correlation with these growth-promoting parameters. Specifically, the SST was observed to reside within the range associated with the maximal growth rate from mid-May to mid-June(Figure 8). This period was punctuated by two significant precipitation events, each characterized by daily totals exceeding 30 mm. These climatic factors together may constitute a crucial part of the environmental recipe that favors the rapid proliferation of the green tide during this interval.

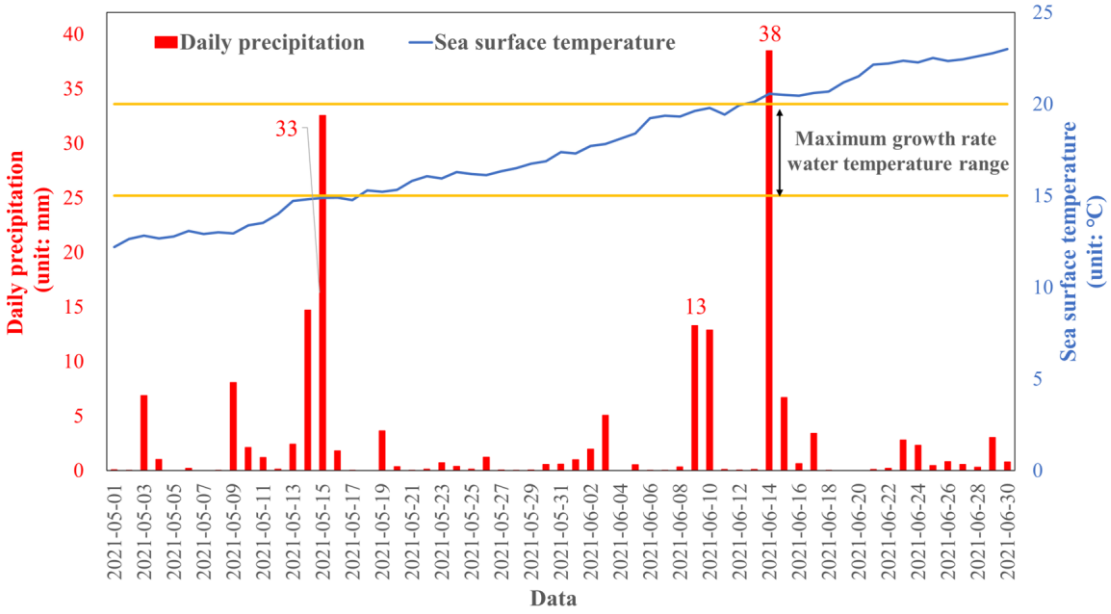

Figure 8. Daily precipitation and SST for 1 May and 30 June 2021.

4. Discussion

In this study, green tide areas monitored from GF-1 data were used to correct the areas derived from MODIS imagery, establishing a linear relationship between the two datasets to enhance the accuracy of green tide area detection in MODIS imagery. However, it is pertinent to note that this linear model may be limited in its applicability during certain stages of the green tide. Specifically, during the early and late stages of green tide when patches are small and dispersed, detecting them with MODIS becomes challenging due to its resolution constraints [9]. MODIS struggles to detect patches smaller than its spatial resolution, and areas less than 11.2 km^2 tend to be underestimated [15]. Given that the linear regression model was based on images from July 10th, coinciding with the peak of the green tide, its suitability may diminish during times when the green tide area is minimal, such as in its initial or fading stages. For the purposes of this study, the model should only be used when the green tide coverage area in MODIS imagery is above 300 km^2. Future research might attempt to expand the model's applicability, aiming for accurate extractions during the initial and decaying stages.

By integrating monthly average sea surface attributes, including temperature, salinity, and precipitation, along with their multi-year monthly averages, and assessing daily SST and precipitation from April to June 2021, certain patterns emerged. Specifically, during this period, the Yellow Sea's northern coastal waters and southern regions exhibited elevated SST and SSS. Such rises in SST and SSS fostered conducive conditions for a massive outbreak of green tide, a phenomenon further exacerbated by concurrent extreme weather

events [46,48]. These climatic conditions could lead to the extensive dispersal of seaweed cultivation rafts into the open sea. The algae attached to these rafts subsequently proliferate substantially in marine environments, serving as a floating seed source. Moreover, during May and June, a pattern of significant rainfall was observed in the northern waters of the Yellow Sea. This precipitation not only facilitates the deposition of atmospheric nutrients such as dissolved inorganic nitrogen and dissolved organic phosphorus but also establishes conditions conducive to the algal blooms such as green tides and red tides. [49,50]. Additionally, it intensifies the seawater convection [46]. This intensified convection results in the upward transport of nutrients from the seabed to the surface, allowing the algae that constitute the algal blooms to uptake these nutrients voraciously. This process may further exacerbate the development and expansion of the algal blooms [51,52]. Our findings also explicitly illustrate an increase in precipitation in 2021 compared to previous years, suggesting that the precipitation variations in 2021 indirectly contributed to the large-scale outbreak of the green tide. Additionally, the correlations between SST, SSS, and rainfall with the changes in the green tide area are 0.43, 0.76, and 0.48, respectively. Based on these correlation values, it is evident that SSS has the highest correlation with the changes in the green tide area. Coupled with the observed increase in salinity levels in 2021 compared to previous years, it can be inferred that the large-scale outbreak of the green tide in 2021 is closely related to SSS.

Continuous advancements in green tide disaster research necessitate the integration of remote sensing imagery of varied resolutions. In this study, only a fusion of GF-1 and MODIS imagery was employed. Although the GF-1 offers relatively high spatial resolution, discrepancies remain with actual conditions. Future investigations might consider incorporating remote sensing data with even higher resolutions for more precise green tide monitoring. Furthermore, the factors leading to a massive green tide outbreak are multifaceted. Subsequent studies on green tide mechanisms might expand their scope, encompassing a broader range of influencing factors for analysis.

5. Conclusions

Utilizing imagery with high spatial and temporal resolutions offers significant advantages for monitoring green tide disasters. To amalgamate the strengths of these two resolutions found in satellite data, this study integrated GF-1 remote sensing imagery with MODIS data, elucidating the distribution characteristics of the 2021 green tide phenomenon. Factors influencing this phenomenon were explored, leading to the following conclusions:

A linear correlation model linking GF-1 and MODIS was established to refine the green tide area monitored using MODIS, enabling a more precise monitoring of the green tide disaster. This provided insights into the distribution range of the green tide over 10 days between May and August 2021, offering a depiction of the drift path of the green tide from its onset in May to its decline in August.

By mid- to late May, green tide emerged in the sea areas near Jiangsu and expanded in a northwest direction. Throughout June, influenced by sea winds and ocean currents, the area engulfed by the green tide progressively enlarged, drifting from Jiangsu to Qingdao in Shandong. By July and August, the green tide was predominantly confined to the coastal areas of Qingdao, and due to human-led cleanup efforts, its presence rapidly diminished.

Several factors contributed to the outbreak of the green tide: initially, extreme weather conditions resulted in algae attached to cultivation rafts dispersing into the sea, serving as a source of seeds; elevated SSTs and SSS in the early stages laid the foundation for the emergence of the green tide; and during its developmental phase, abundant rainfall created optimal conditions for the proliferation of the green tide. Among the correlations between SST, SSS, and precipitation within the green tide area, SSS exhibited the highest correlation, with a value of 0.76.

Author Contributions: Conceptualization, Y.M. (Yanzhuo Men) and Y.Z.; methodology, Y.M. (Yanzhuo Men); software, J.Y.T.; validation, Y.L., K.P.W. and Y.Z.; formal analysis, Y.M. (Yanzhuo Men) and Y.L.;

investigation, Y.M. (Yufei Ma); resources, J.Y.T.; data curation, Y.M. (Yanzhuo Men); writing—original draft preparation, Y.M. (Yanzhuo Men); writing—review and editing, J.Y.T. and Y.Z.; visualization, Y.M. (Yufei Ma); supervision, Y.Z.; project administration, Y.Z.; funding acquisition, Y.Z. All authors have read and agreed to the published version of the manuscript.

Funding: This research was funded by the National Natural Science Foundation (U1901215), the Marine Special Program of Jiangsu Province in China (JSZRHYKJ202007), and the Natural Scientific Foundation of Jiangsu Province (BK20181413).

Institutional Review Board Statement: Not applicable.

Informed Consent Statement: Not applicable.

Data Availability Statement: Data are contained within the article.

Acknowledgments: The authors are grateful to the China National High-resolution Earth Observation System and NASA for providing the GF-1 and MODIS satellite-based remote sensing data, respectively. The data from ERA5, COOS, and SMAP are also highly appreciated.

Conflicts of Interest: The authors declare no conflict of interest.

References

1. Zhou, M.-J.; Shen, Z.-L.; Yu, R.-C. Responses of a coastal phytoplankton community to increased nutrient input from the Changjiang (Yangtze) River. *Cont. Shelf Res.* **2008**, *28*, 1483–1489. [CrossRef]
2. Xing, Q.; Hu, C. Mapping macroalgal blooms in the Yellow Sea and East China Sea using HJ-1 and Landsat data: Application of a virtual baseline reflectance height technique. *Remote Sens. Environ.* **2016**, *178*, 113–126. [CrossRef]
3. Liu, D.; Keesing, J.K.; Dong, Z.; Zhen, Y.; Di, B.; Shi, Y.; Fearns, P.; Shi, P. Recurrence of the world's largest green-tide in 2009 in Yellow Sea, China: Porphyra yezoensis aquaculture rafts confirmed as nursery for macroalgal blooms. *Mar. Pollut. Bull.* **2010**, *60*, 1423–1432. [CrossRef]
4. Hu, L.; Hu, C.; Ming-Xia, H. Remote estimation of biomass of Ulva prolifera macroalgae in the Yellow Sea. *Remote Sens. Environ.* **2017**, *192*, 217–227. [CrossRef]
5. Hu, L.; Zeng, K.; Hu, C.; He, M.-X. On the remote estimation of Ulva prolifera areal coverage and biomass. *Remote Sens. Environ.* **2019**, *223*, 194–207. [CrossRef]
6. Shang, W.; Gao, Z.; Jiang, X.; Liu, C.; Gao, W. *Green Tide Disaster Monitoring System Based on Multi-Source Data*; SPIE: Bellingham, DC, USA, 2016; Volume 9975.
7. Shang, W.; Gao, Z.; Gao, M.; Jiang, X. Monitoring Green Tide in the Yellow Sea Using High-Resolution Imagery and Deep Learning. *Remote Sens.* **2023**, *15*, 1101. [CrossRef]
8. Cui, B.; Zhang, H.; Jing, W.; Liu, H.; Cui, J. SRSe-Net: Super-Resolution-Based Semantic Segmentation Network for Green Tide Extraction. *Remote Sens.* **2022**, *14*, 710. [CrossRef]
9. Cui, T.-W.; Zhang, J.; Sun, L.-E.; Jia, Y.-J.; Zhao, W.; Wang, Z.-L.; Meng, J.-M. Satellite monitoring of massive green macroalgae bloom (GMB): Imaging ability comparison of multi-source data and drifting velocity estimation. *Int. J. Remote Sens.* **2012**, *33*, 5513–5527. [CrossRef]
10. Xiao, Y.; Zhang, J.; Cui, T. High-precision extraction of nearshore green tides using satellite remote sensing data of the Yellow Sea, China. *Int. J. Remote Sens.* **2017**, *38*, 1626–1641. [CrossRef]
11. Adjovu, G.E.; Stephen, H.; James, D.; Ahmad, S. Overview of the Application of Remote Sensing in Effective Monitoring of Water Quality Parameters. *Remote Sens.* **2023**, *15*, 1938. [CrossRef]
12. Klemas, V. Remote sensing of algal blooms: An overview with case studies. *J. Coast. Res.* **2012**, *28*, 34–43. [CrossRef]
13. Wu, X.; Xu, Q.; Li, G.; Liou, Y.-A.; Wang, B.; Mei, H.; Tong, K. Remotely-Observed Early Spring Warming in the Southwestern Yellow Sea Due to Weakened Winter Monsoon. *Remote Sens.* **2019**, *11*, 2478. [CrossRef]
14. Ma, Y.; Wong, K.; Tsou, J.Y.; Zhang, Y. Investigating spatial distribution of green-tide in the Yellow Sea in 2021 using combined optical and SAR images. *J. Mar. Sci. Eng.* **2022**, *10*, 127. [CrossRef]
15. Yang, D.; Yuen, K.-V.; Gu, X.; Sun, C.; Gao, L. Influences of environmental factors on the dissipation of green tides in the Yellow Sea, China. *Mar. Pollut. Bull.* **2023**, *189*, 114737. [CrossRef] [PubMed]
16. Zhang, Y.; He, P.; Li, H.; Li, G.; Liu, J.; Jiao, F.; Zhang, J.; Huo, Y.; Shi, X.; Su, R. Ulva prolifera green-tide outbreaks and their environmental impact in the Yellow Sea, China. *Neurosurgery* **2019**, *6*, 825–838. [CrossRef]
17. Lee, J.H.; Pang, I.C.; Moon, I.J.; Ryu, J.H. On physical factors that controlled the massive green tide occurrence along the southern coast of the Shandong Peninsula in 2008: A numerical study using a particle-tracking experiment. *J. Geophys. Res. Ocean.* **2011**, *116*, 1–12. [CrossRef]
18. Cao, H.; Han, L. Drift path of green tide and the impact of typhoon "Chan-hom" in the Chinese Yellow Sea based on GOCI images in 2015. *Ecol. Inform.* **2020**, *60*, 101156. [CrossRef]
19. Li, D.; Gao, Z.; Song, D. Analysis of environmental factors affecting the large-scale long-term sequence of green tide outbreaks in the Yellow Sea. *Estuar. Coast. Shelf Sci.* **2021**, *260*, 107504. [CrossRef]

20. Li, D.; Gao, Z.; Wang, Z. Analysis of the reasons for the outbreak of Yellow Sea green tide in 2021 based on long-term multi-source data. *Mar. Environ. Res.* **2022**, *178*, 105649. [CrossRef]
21. Li, D.; Gao, Z.; Xu, F. Research on the dissipation of green tide and its influencing factors in the Yellow Sea based on Google Earth Engine. *Mar. Pollut. Bull.* **2021**, *172*, 112801. [CrossRef]
22. Xu, F.; Zheng, X.; Gao, Z.; Song, D.; Chen, M. Multi-resource data-based research on remote sensing monitoring over the green tide in the Yellow Sea. In Proceedings of the Remote Sensing & Modeling of Ecosystems for Sustainability XIV, San Diego, CA, USA, 1 September 2017.
23. Zheng, X.; Gao, Z.; Ning, J.; Xu, F.; Liu, C.; Sun, Z. *Remote Sensing Monitoring of Green Tide in the Yellow Sea in 2015 Based on GF-1 WFV Data*; SPIE: Bellingham, DC, USA, 2016; Volume 9975.
24. Li, D.; Gao, Z.; Song, D.; Shang, W.; Jiang, X. Characteristics and influence of green tide drift and dissipation in Shandong Rongcheng coastal water based on remote sensing. *Estuar. Coast. Shelf Sci.* **2019**, *227*, 106335. [CrossRef]
25. Li, L.; Zheng, X.; Wei, Z.; Zou, J.; Xing, Q. A Spectral-Mixing Model for Estimating Sub-Pixel Coverage of Sea-Surface Floating Macroalgae. *Atmos. -Ocean* **2018**, *56*, 296–302. [CrossRef]
26. Xu, F.; Gao, Z.; Ning, J.; Zheng, X.; Liu, C.; Gao, W. *Error Analysis on Green Tide monitoring using MODIS Data in the Yellow Sea Based on GF-1 WFV Data*; SPIE: Bellingham, DC, USA, 2016; Volume 9975.
27. Rouse, J.W.; Haas, R.H.; Schell, J.A.; Deering, D.W. Monitoring vegetation systems in the Great Plains with ERTS. *NASA Spec. Publ.* **1974**, *351*, 309.
28. Yu, H.; Lee, J.-Y.; Lee, W.-K.; Cui, G.; Cho, J.-K.; Wei, G.; Li, L. Application of CASI Hyperspectral Image to Analysis of the Distribution of Hydrogen-Fluoride-Damaged Vegetation in Gumi, Korea. *J. Indian Soc. Remote Sens.* **2017**, *45*, 317–326. [CrossRef]
29. Keesing, J.K.; Liu, D.; Fearns, P.; García, R. Inter- and intra-annual patterns of Ulva prolifera green tides in the Yellow Sea during 2007-2009, their origin and relationship to the expansion of coastal seaweed aquaculture in China. *Mar. Pollut. Bull.* **2011**, *62*, 1169–1182. [CrossRef] [PubMed]
30. Xing, Q.; Zheng, X.-Y.; Shi, P.; Hao, J.; Yu, D.; Liang, S.; Liu, D.; Zhang, Y.-Z. Monitoring "green tide" in the Yellow Sea and the East China Sea using multi-temporal and multi-source remote sensing images. *Guang Pu Xue Yu Guang Pu Fen Xi* **2011**, *31*, 1644–1647.
31. Sakib, M.H.; Rashid, H.; Yang, C.-S. Comparing performance of inter-sensor NDVI for the detection of floating macroalgal blooms in the Yellow Sea. *Indian J. Geo-Mar. Sci.* **2021**, *50*, 613–619.
32. Wang, Z.; Fang, Z.; Wu, Y.; Liang, J.; Song, X. Multi-Source Evidence Data Fusion Approach to Detect Daily Distribution and Coverage of Ulva Prolifera in the Yellow Sea, China. *IEEE Access* **2019**, *7*, 115214–115228. [CrossRef]
33. Cui, T.; Liang, X.; Gong, J.; Tong, C.; Xiao, Y.; Liu, R.; Zhang, X.; Zhang, J. Assessing and refining the satellite-derived massive green macro-algal coverage in the Yellow Sea with high resolution images. *ISPRS J. Photogramm. Remote Sens.* **2018**, *144*, 315–324. [CrossRef]
34. Zhang, J.H.; Huo, Y.Z.; Zhang, Z.L.; Yu, K.F.; He, Q.; Zhang, L.H.; Yang, L.L.; Xu, R.; He, P.M. Variations of morphology and photosynthetic performances of Ulva prolifera during the whole green tide blooming process in the Yellow Sea. *Mar. Environ. Res.* **2013**, *92*, 35–42. [CrossRef]
35. Li, Y.; Song, W.; Xiao, J.; Wang, Z.; Fu, M.; Zhu, M.; Li, R.; Zhang, X.; Wang, X. Tempo-spatial distribution and species diversity of green algae micro-propagules in the Yellow Sea during the large-scale green tide development. *Harmful Algae* **2014**, *39*, 40–47. [CrossRef]
36. Zhou, F.; Ge, J.; Liu, D.; Ding, P.; Chen, C.; Wei, X. The Lagrangian-based floating macroalgal growth and drift model (FMGDM v1. 0): Application to the Yellow Sea green tide. *Geosci. Model Dev.* **2021**, *14*, 6049–6070. [CrossRef]
37. Qingdao Municipal Ocean Development Bureau. Stay True to the Original Aspiration, Take on the Mission Courageously, Anchor the Goal, and Strive Forward. 2021. Available online: https://ocean.qingdao.gov.cn/gzdt/202110/t20211030_23701888.shtml (accessed on 24 February 2023).
38. Department of Marine Early Warning and Monitoring. *China Marine Disaster Bulletin 2022*; Ministry of Natural Resources: Beijing, China, 2021.
39. Chen, Z.; Liu, M.; Yang, Y.; Bi, M.; Li, M.; Liu, W. Environmental and economic impacts of different disposal options for ulva prolifera green tide in the yellow Sea, China. *ACS Sustain. Chem. Eng.* **2022**, *10*, 11483–11492. [CrossRef]
40. Qi, L.; Hu, C.; Barnes, B.B.; Lapointe, B.E.; Chen, Y.; Xie, Y.; Wang, M. Climate and anthropogenic controls of seaweed expansions in the East China Sea and Yellow Sea. *Geophys. Res. Lett.* **2022**, *49*, e2022GL098185. [CrossRef]
41. Cohen, R.A.; Fong, P. Physiological responses of a bloom-forming green macroalga to short-term change in salinity, nutrients, and light help explain its ecological success. *Estuaries* **2004**, *27*, 209–216. [CrossRef]
42. Lin, A.P.; Wang, C.; Pan, G.H.; Song, L.Y.; Gao, S.; Xie, X.J.; Wang, Z.Y.; Niu, J.F.; Wang, G.C. Diluted seawater promoted the green tide of Ulva prolifera (Chlorophyta, Ulvales). *Phycol. Res.* **2011**, *59*, 295–304. [CrossRef]
43. Mamboya, F.; Lyimo, T.J.; Landberg, T.; Björk, M. Influence of combined changes in salinity and copper modulation on growth and copper uptake in the tropical green macroalga Ulva reticulata. *Estuar. Coast. Shelf Sci.* **2009**, *84*, 326–330. [CrossRef]
44. Wang, Z.; Xiao, J.; Fan, S.; Li, Y.; Liu, X.; Liu, D. Who made the world's largest green tide in China?—An integrated study on the initiation and early development of the green tide in Yellow Sea. *Limnol. Oceanogr.* **2015**, *60*, 1105–1117. [CrossRef]

45. Schories, D.; Anibal, J.; Chapman, A.S.; Herre, E.; Isaksson, I.; Lillebø, A.I.; Pihl, L.; Reise, K.; Sprung, M.; Thiel, M. Flagging greens: Hydrobiid snails as substrata for the development of green algal mats (*Entero-morpha* spp.) on tidal flats of North Atlantic coasts. *Mar. Ecol. Prog. Ser.* **2000**, *199*, 127–136. [CrossRef]
46. Zhang, G.; Zhang, J.; Liu, S. Characterization of nutrients in the atmospheric wet and dry deposition observed at the two monitoring sites over Yellow Sea and East China Sea. *J. Atmos. Chem.* **2007**, *57*, 41–57. [CrossRef]
47. Taylor, R.; Fletcher, R.; Raven, J. Preliminary studies on the growth of selected 'green tide'algae in laboratory culture: Effects of irradiance, temperature, salinity and nutrients on growth rate. *Bot. Mar.* **2001**, *44*, 327–336. [CrossRef]
48. Zhang, G.; Wu, M.; Zhang, A.; Xing, Q.; Zhou, M.; Zhao, D.; Song, X.; Yu, Z. Influence of Sea Surface Temperature on Outbreak of Ulva prolifera in the Southern Yellow Sea, China. *Chin. Geogr. Sci.* **2020**, *30*, 631–642. [CrossRef]
49. Zhang, H.; Su, R.; Shi, X.; Zhang, C.; Yin, H.; Zhou, Y.; Wang, G. Role of nutrients in the development of floating green tides in the Southern Yellow Sea, China, in 2017. *Mar. Pollut. Bull.* **2020**, *156*, 111197. [CrossRef]
50. Chongrong, Z.; Guangyi, L.; Jingwi, C.; Baoqing, L.; Fan, Y.; Rui, Y. Potential Effects of Some Environmental Factors on a Dinoflagellate Red Tide Caused by Gymnodinium cat-enatum in Shenhu Bay in 2017. *Meteorol. Environ. Res.* **2019**, *10*, 30–34.
51. Van Alstyne, K.L.; Nelson, T.A.; Ridgway, R.L. Environmental Chemistry and Chemical Ecology of "Green Tide" Seaweed Blooms. *Integr. Comp. Biol.* **2015**, *55*, 518–532. [CrossRef] [PubMed]
52. Wang, S.; Zhao, L.; Wang, Y.; Zhang, H.; Li, F.; Zhang, Y. Distribution characteristics of green tides and its impact on environment in the Yellow Sea. *Mar. Environ. Res.* **2022**, *181*, 105756. [CrossRef] [PubMed]